minerals

MDPI

Article

Effect of Al Substitution on Visible Short-Wave Infrared Reflectance Spectroscopy (VSWIR) of Goethite and Ferrihydrite

Keyan Chen [1,2,3], Xiaorong Qin [1,2,3], Jingwen Zhou [1,2,3], Wei Tan [1,2,*], Xiaoliang Liang [1,2], Hongping He [1,2,3], Jianxi Zhu [1,2], Mengqi Han [1,2,3] and Lianying Luo [1,2,3]

1 CAS Key Laboratory of Mineralogy and Metallogeny/Guangdong Provincial Key Laboratory of Mineral Physics and Materials, Guangzhou Institute of Geochemistry, Chinese Academy of Sciences, Guangzhou 510640, China; chenkeyan@gig.ac.cn (K.C.); qinxiaorong@gig.ac.cn (X.Q.); zhoujingwen@gig.ac.cn (J.Z.); liangxl@gig.ac.cn (X.L.); hehp@gig.ac.cn (H.H.); zhujx@gig.ac.cn (J.Z.); hanmengqi23@mails.ucas.ac.cn (M.H.); luolianying@gig.ac.cn (L.L.)
2 CAS Center for Excellence in Deep Earth Science, Guangzhou 510640, China
3 University of Chinese Academy of Sciences, Beijing 100049, China
* Correspondence: tanwei@gig.ac.cn

Abstract: Goethite and ferrihydrite are the two major iron hydroxides, essential mineral constituents in the terrestrial surface system. Aluminum (Al) is the most common substituent in iron hydroxides, and it may significantly change the bulk and surficial physicochemical properties of iron hydroxides. Consequently, a practical and convenient approach is needed to efficiently identify the Al substitution degrees of iron hydroxides in natural occurrences. This study presents a comprehensive investigation of the VSWIR characteristics of laboratory-synthesized Al-substituted goethite and ferrihydrite, to establish diagnostic VSWIR parameters for the identification and quantification of Al substitution levels in iron hydroxides. The findings revealed that Al substitution can affect the band positions (P) of goethite and ferrihydrite at ~650 nm, ~900 nm, and ~1400 nm. The relationships between the Al substitution of ferrihydrite and VSWIR parameters can be expressed as P900 = $-0.43 \times$ Al(%) + 931 and P1400 = $-0.07 \times$ Al(%) + 1428, while that of goethite can be expressed as P650 = $0.42 \times$ Al(%) + 657 and P900 = $2.29 \times$ Al(%) + 936. The peak fitting results showed that the absorption intensity at 480–550 nm linearly decreases with increased Al substitution. The obtained VSWIR spectra of Al-substituted goethite and ferrihydrite provide a critical supplement to the spectral library for (Al) iron hydroxides, and these VSWIR parameters can be utilized for the semi-quantitative determination of Al substitution in natural iron hydroxides

Keywords: goethite; ferrihydrite; Al substitution; VSWIR parameter

check for updates

Citation: Chen, K.; Qin, X.; Zhou, J.; Tan, W.; Liang, X.; He, H.; Zhu, J.; Han, M.; Luo, L. Effect of Al Substitution on Visible Short-Wave Infrared Reflectance Spectroscopy (VSWIR) of Goethite and Ferrihydrite. *Minerals* **2024**, *14*, 618. https://doi.org/10.3390/min14060618

Academic Editor: Bernard Hubbard

Received: 19 February 2024
Revised: 15 June 2024
Accepted: 16 June 2024
Published: 18 June 2024

Copyright: © 2024 by the authors. Licensee MDPI, Basel, Switzerland. This article is an open access article distributed under the terms and conditions of the Creative Commons Attribution (CC BY) license (https://creativecommons.org/licenses/by/4.0/).

1. Introduction

Ferrihydrite ($Fe_{10}O_{14}(OH)_2 \cdot nH_2O$) and goethite ($\alpha$-FeOOH) are ubiquitous iron hydroxides in soils and sediments that are sensitive to climatic and environmental changes on Earth [1–3]. Ferrihydrite serves as an essential precursor for hematite and goethite. In natural occurrences, goethite is primarily formed through the dissolution and re-precipitation of ferrihydrite [1,4,5]. Goethite occurs predominantly in cool humid climates, while hematite formation is favored in warmer, subtropical and tropical climates [1,5–7]. Therefore, hematite and goethite concentrations, as well as their relative abundances, have been used widely as indicators of soil moisture regimes and pedogenic processes, which are in turn related to climate variability [4,8–11]. In addition, the relative proportion of hematite and goethite has been viewed as an effective indicator of the groundwater table, dividing a regolith into two sections with distinctive hydrological conditions [10–12].

Many trivalent metal cations with smaller radii, e.g., Al^{3+}, Mn^{3+}, and Cr^{3+}, can substitute the octahedral-coordinated Fe^{3+} of ferrihydrite and goethite [1]. Among them, Al substitution in iron hydroxides is most common in tropical soils, especially in warm

and humid environments [1,2]. For goethite, as much as 33% of Fe^{3+} can be replaced by Al^{3+} [1]. Ferrihydrite exhibits a maximum Al substitution of 25% [13]. Al substitution is thermodynamically favored in ferrihydrite compared to goethite [14–16]. As Al substitution may cause significant changes in the bulk and surficial physicochemical properties of iron hydroxides, it is essential to develop techniques to determine the level of Al substitution. Previous studies have used X-ray diffraction (XRD) [17], Mössbauer spectroscopy [18], Raman spectroscopy [19,20], Fourier transform infrared (FTIR) spectroscopy [21], and transmission electron microscopes [20,22] to characterize the effects of aluminum substitution in ferrihydrite and goethite. However, those laboratory-based instruments are essentially time-consuming and costly, and inefficient in the composition analysis of abundant natural samples in the field.

Visible-shortwave infrared reflectance (VSWIR) spectroscopy is a rapid, portable, and economical technique [12,23–25]. VSWIR can also be employed as a tool for mineral mapping, with promising applications in the HyMap airborne hyperspectral scanner [26]. As of now, many studies focus on the VSWIR spectral characteristics of Al-substituted hematite [14]. However, an explicit understanding of the VSWIR spectral features of Al-substituted goethite and ferrihydrite is still lacking. In this study, X-ray diffraction (XRD) was employed for phase identification of the synthesized samples, SEM and TEM images were utilized to observe the morphology features and particle-size distribution of the samples, and a thermal gravimetric analyzer (TG) was employed to quantify the variations in structural hydroxyl and water. Our study demonstrates that VSWIR spectroscopy is feasible for identifying and quantifying Al substitution in goethite and ferrihydrite, which is helpful in the reconstruction of the paleoenvironmental and hydrological conditions of soils and sediments.

2. Materials and Methods

2.1. Samples Preparation

2.1.1. Preparation of Al-goethite

Al-substituted goethite was synthesized according to Cornell [1] and Böhm [27]. A total of 100 mL of 1 mol/L $Fe(NO_3)_3{\cdot}9H_2O$ and $Al(NO_3)_3{\cdot}9H_2O$ was mixed in a 2 L polyethylene flask, then 180 mL of 5M KOH was added and stirred rapidly. The suspension was immediately diluted to 2 L with distilled water and was held in a closed polyethylene flask at 70 °C for 60 h. At this stage, the voluminous, red-brown suspension of ferrihydrite was converted to a compact, yellow-brown precipitate of goethite. The synthesized sample was then centrifuged, washed, and dried. Based on the molar ratio of Al and Fe in the starting material (Al/(Al+Fe) = 0%, 5%, 10%, 15%, 20%, and 30%), the samples were designated as G-0, G-5, G-10, G-15, G-20, and G-30 (Table 1).

Table 1. Al substitution of synthesized goethite (G) and ferrihydrite (F).

Sample [1]	Al Content in Starting Material (mol %)	Al Substitution in Final Samples (mol %)
G-0	0	0.0
G-5	5.0	1.9
G-10	10.0	3.1
G-15	15.0	4.9
G-20	20.0	8.5
G-30	30.0	11.2
F-0	0	0.1
F-5	5.0	5.2
F-10	10.0	10.7
F-15	15.0	16.2
F-20	20.0	21.4
F-25	25.0	26.7
F-30	30.0	31.8

[1] Specimen numbers correspond to the initial Al substitution (Al/(Fe+Al) mol %).

2.1.2. Preparation of Al-ferrihydrite

Al-substituted ferrihydrite was synthesized in the laboratory as reported by [1]. At 25°C, different proportions and a total amount of 0.1 mol of $Fe(NO_3)_3 \cdot 9H_2O$ and $Al(NO_3)_3 \cdot 9H_2O$ was taken in a plastic beaker and dissolved in 500 mL of deionized water. A 1 mol/L KOH solution was added to the solution at a rate of 10 mL/min, until the pH stabilized at 7.50 ± 0.05. After being stirred for 30 min, the suspension was centrifuged at 11,000 r/min for 5 min. The synthesized product was washed 4–5 times with distilled water until the conductivity was < 4 uS/m. After being washed, the samples were freeze-dried at −40 °C for 24 h. According to the molar ratio of Al and Fe in the starting material (Al/(Al+Fe) = 0%, 5%, 10%, 15%, 20%, 25%, and 30%), the samples were designated as F-0, F-5, F-10, F-15, F-20, F-25, and F-30 (Table 1).

2.2. Analytical Methods

2.2.1. X-ray Diffraction (XRD)

To investigate the mineral composition and Al substitution degrees of iron hydroxides in the synthesized sample, XRD analyses were conducted using the Rigaku MiniFlex-400 X-ray diffractometer (Tokyo, Japan) at the Key Laboratory of Mineralogy and Metallogeny, Guangzhou Institute of Geochemistry, Chinese Academy of Sciences. The diffractometer is equipped with a Hybrid pixel array detector, a Cu source, and a Ni filter. The diffractometer functions under a current of 15 mA and a voltage of 40 kV. All samples were prepared by firmly pressing ground powder materials in the slides for bulk powder mounting. The XRD patterns were recorded between 3° and 80° (2θ) at a scanning speed of 10°/min and a step size of 0.01°.

2.2.2. Thermal Gravimetric Analyzer (TG)

Since Al substitution possibly leads to changes in the OH content of iron hydroxides, TG analyses were used to quantify the OH content in the samples, which should be coincident with the changes in the VSWIR absorption bands at ~1400 nm and ~1900 nm. Thermogravimetric analysis (TG) is a technique that measures the physical properties and temperature relationships of a substance under programmatically controlled temperature conditions. In this study, the Al-substitution goethite and ferrihydrite samples were subjected to continuous heating at a uniform rate (10 °C/min) in a nitrogen (N_2) environment at 30 °C. The highest temperature reached was 1000 °C, and the weight loss during this heating process was monitored.

2.2.3. Scanning Electron Microscope (SEM)

A SEM was used to investigate the morphology and size features of the synthesized goethite with different degrees of Al substitution. Less than 1 mg of the sample was mixed with 10 mg of ultrapure water and sonicate to obtain a uniformly dispersed colloidal-like substance. The suspension was dropped onto a carbon film and evaporated at room temperature for SEM investigation. The morphology and size features of the samples were investigated using the Focused Ion Beam Scanning Electron Microscope (FEI Helios 5CX) (Czech Republic, Thermo Fisher Scientific Brno s.r.o) at the Key Laboratory of Mineralogy and Metallogeny, Guangzhou Institute of Geochemistry, Chinese Academy of Sciences. The microscope is equipped with a through-lens detection (TLD) electron detector capable of secondary electron and backscattered electron modes.

2.2.4. Transmission Electron Microscope (TEM)

The morphology, particle size, and semi-quantitative Al content of nano-sized Al-substituted iron hydroxides were analyzed using a high-resolution transmission electron microscope (HRTEM). First, ~1 mg of sample was mixed with ~2 mL of anhydrous ethanol. The mixture was ultrasonicated for 10 min to ensure thorough dispersion. Subsequently, a small amount of the dispersed solution was dropped onto a copper grid coated with a clean carbon film. The grid was then tested after the evaporation and drying of the

solution. HRTEM observation was performed on an FEI Talos F200S microscope (Brno, Czech Republic) equipped with an X-ray energy-dispersive detector at the Key Laboratory of Mineralogy and Metallogeny, Guangzhou Institute of Geochemistry, Chinese Academy of Sciences. The instrument was operated at an accelerating voltage of 200 kV.

2.2.5. Visible-Shortwave Infrared Reflectance (VSWIR) Spectroscopy

This study performed a spectra separation analysis [28,29] on the VSWIR spectra from 350 to 1400 nm associated with different energy electron transitions of Fe^{3+} cations in iron hydroxides. The synthesized Al-substituted iron hydroxides were measured using an Analytical Spectral Devices (ASD) TerraSpec4 Hi-Res spectrometer (Holland, Malvern Panalytical Ltd) with a spot size of approximately 20 mm. The spectral resolution is 3 nm (Full-Width–Half-Maximum) at 700 nm, 10 nm at 1400 nm, and 10 nm at 2100 nm. The sampling interval is 1.4 nm for the spectral region 350–1000 nm, and 2 nm for the spectral region 1000–2500 nm. During data collection, 200 scan acquisitions were set to yield an average spectrum for each measured spectrum, to improve the signal-to-noise ratio.

ASD spectral files were processed using ViewSpecPro (version 6.0) software. The VSWIR spectra of ferrihydrite and goethite with different Al substitution degrees in the 350–1350 nm range were subjected to continuous smoothing, continuum removal, and second-order derivative preprocessing. The position of absorptions at around 650 nm (P650), 900 nm (P900), and1400 nm (P1400) were defined by the position of the reflectance minimum from 600 to 700 nm, 800 to 1000 nm, and 1350 to 1450 nm [30]. The position of each absorption band was calculated using the symmetric peak pair positions resolved and identified by the residual peak-fitting method with PeakFit (version 4.12). The peak type selection includes "Spectroscopy" and "Gauss + Lorenz Area". The fitting process proceeded until a maximum R^2 and a minimum residual of random distribution were reached.

3. Results

3.1. Morphological Characteristics of Synthetic Iron Hydroxides

3.1.1. Ferrihydrite

The TEM images show that the synthesized ferrihydrite generally presents as amorphous aggregate. The series of Al-substituted ferrihydrite nanoparticles show poorly defined edges and indiscernible lattice fringes (Figure 1). The observed minimum particle size is approximately 5–10 nm, and no significant changes in particle size are observed with increasing Al substitution (Figure 1).

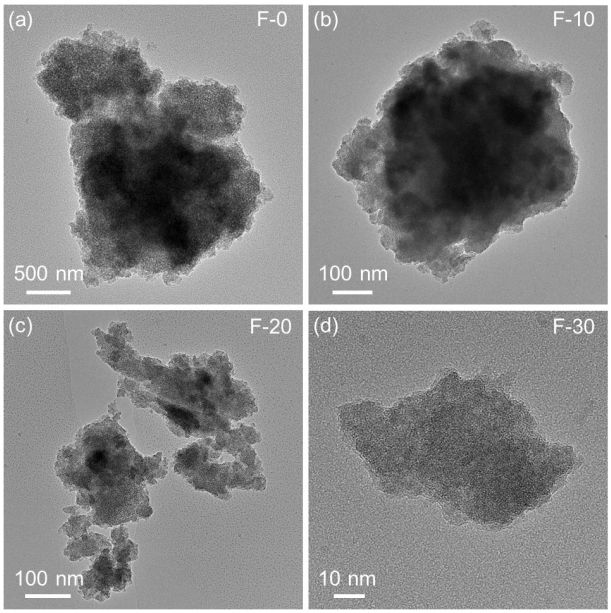

Figure 1. TEM images of F-0, F-10, F-20, and F-30 (**a**–**d**).

3.1.2. Goethite

The SEM and TEM images showed systematic changes in the morphologies of the synthesized goethite with increasing degrees of Al substitution. It is evident that the G-0 goethite crystals exhibit an elongated needle-like shape, with a relatively high degree of size dispersion. As the Al substitution increases, the crystal length gradually decreases from ~1370 nm to ~350 nm, and the crystal diameter gradually decreases from ~189 nm to ~105 nm. The crystal morphology of goethite changes from long needle-like to short columnar with increasing Al substitution (Figure 2a–f).

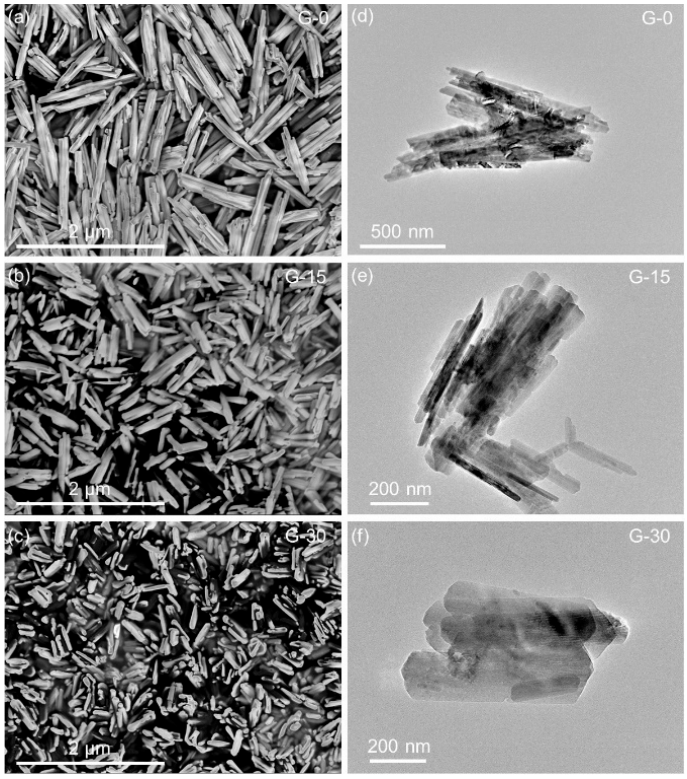

Figure 2. SEM (**a**–**c**), and TEM (**d**–**f**) images of G-0, G-15, and G-30.

The size and aspect ratios of approximately 150 particles for each sample in the goethite series were measured using Image J software. G-0 goethite displayed a relatively high degree of size variation, which likely gradually decreased with an increasing level of Al substitution. The results showed that the average lengths (L) of G-0, G-15, and G-30 are 1371 ± 383 nm, 477 ± 124 nm, and 353 ± 78 nm, respectively, while the average diameters (D) are 189 ± 52 nm, 111 ± 25 nm, and 105 ± 24 nm, respectively. The aspect ratios (L/D) of crystal particles are 7.66 ± 2.46, 4.48 ± 1.47, and 3.50 ± 0.92, respectively (Figure 3a–c).

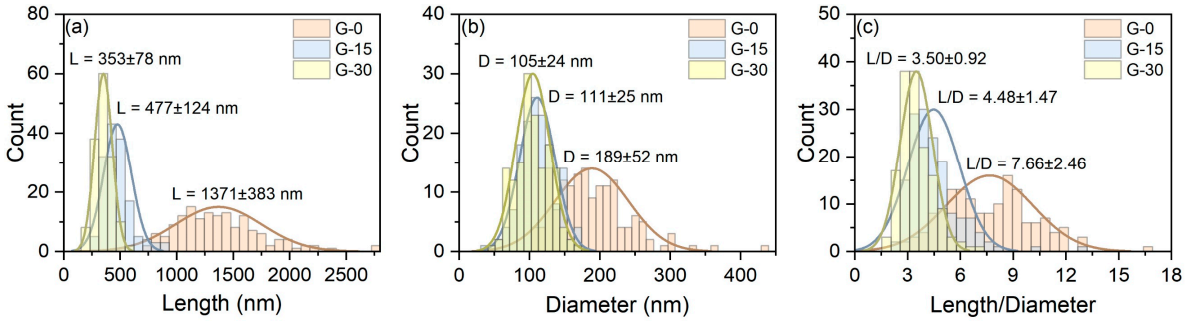

Figure 3. Distribution images of length (**a**), diameter (**b**), and length–diameter ratio (**c**) of synthesized goethite in Figure 2a–c using particle size statistics.

3.2. Crystallographic Characteristics of Synthetic Iron Hydroxides

3.2.1. Ferrihydrite

The XRD patterns of Al-substituted ferrihydrite are shown in Figure 4. All the samples display two broad characteristic peaks at 35° and 62°, corresponding to standard ferrihydrite (PDF#29-0712). The broad and weak nature of the diffraction peaks is consistent with the characteristics of low crystallinity of small-sized ferrihydrite [1]. The positions and intensities of the diffraction at 35° and 62° do not exhibit significant differences for ferrihydrite with different degrees of Al substitution.

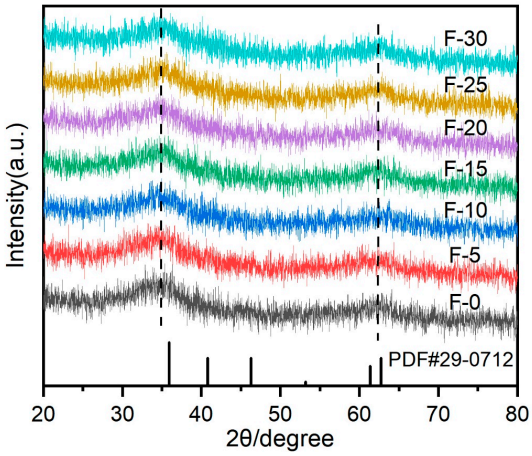

Figure 4. XRD pattern of Al-substituted ferrihydrite.

3.2.2. Goethite

All the samples display characteristic diffraction peaks (Figure 5a) corresponding to standard goethite (PDF#81-0463). The diffraction peaks other than goethite can be hardly discerned, demonstrating the absence of other mineral phases in the samples. The sharp diffraction peaks of all the goethite samples are indicative of good crystallinity. Given that Al^{3+} (0.53 Å) has a smaller ionic radius relative to Fe^{3+} (0.65 Å), characteristic diffraction peaks of the crystal plane, such as (110), (130), (021), (221), and (151), show a tendency to shift towards higher 2θ angles (Figure 5b,c), suggesting a gradual decrease in the interplanar spacing of these crystallographic planes in goethite with increasing Al substitution.

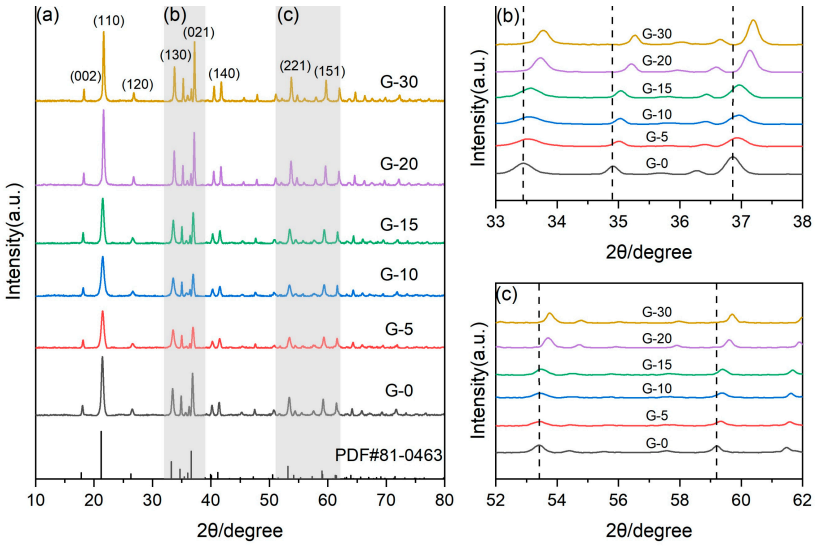

Figure 5. (**a**) XRD pattern of Al-substituted goethite; (**b**,**c**) enlarged XRD patterns of regions from gray rectangle in (**a**).

3.3. Hydroxyl (Metal–OH) Contents in Synthetic Iron Hydroxides

3.3.1. Ferrihydrite

The TG and its derivative curves (DTG) for F-0, F-5, F-10, F-15, F-20, F-25, and F-30 are shown in Figure 6a. A distinct weight loss peak is observed in the range of 75–150 °C, indicating the presence of a significant amount of adsorbed water on the surface of the ferrihydrite. As the temperature continues to rise beyond 150 °C, a gradual and continuous weight loss is observed, suggesting different stabilities of surface hydroxyls, structural hydroxyls, and structural water with varying decomposition temperatures [31]. After being heated to 150 °C, the weight losses for F-0, F-5, F-10, F-15, F-20, F-25, and F-30 are 12.61%, 17.49%, 12.73%, 13.47%, 13.68%, 13.36%, and 15.17%, respectively. Upon being heated from 150 °C to 800 °C, the weight losses for the seven samples are 7.66%, 8.50%, 10.03%, 10.25%, 11.66%, 13.18%, and 13.97%, respectively. Overall, ferrihydrite tends to have more structural hydroxyl and water with increasing degrees of Al substitution (Figure 6a).

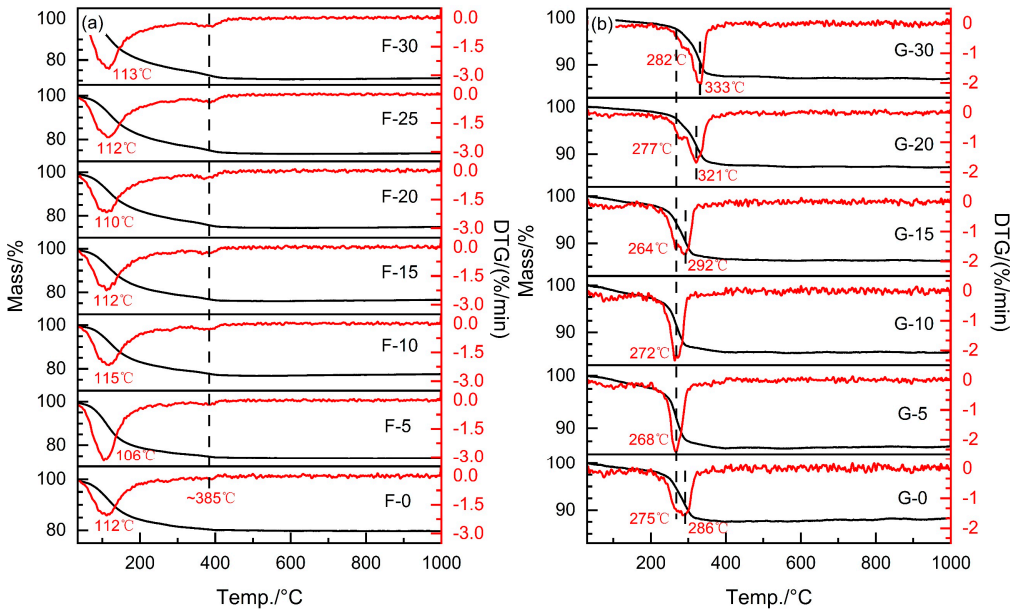

Figure 6. TG and DTG curves of Al-substituted ferrihydrite (**a**) and Al-substituted goethite (**b**). The red line is the curve of DTG and the black line is the curve of TG.

3.3.2. Goethite

The thermogravimetric analysis (TG) and its derivative curves for G-0, G-5, G-10, G-15, G-20, and G-30 are shown in Figure 6b. As the temperature increases, the Al-substituted goethite sequentially loses weakly bound adsorbed water (<150 °C) and more strongly bound hydroxyl and structural water (>150 °C), resulting in a continuous weight loss [31]. After being heated to 150 °C, the weight losses for G-0, G-5, G-10, G-15, G-20, and G-30 are 1.30%, 1.57%, 1.91%, 1.36%, 0.61%, and 0.81%, respectively. Upon being heated from 150 °C to 800 °C, the weight losses for the six samples are 10.72%, 11.95%, 12.26%, 12.28%, 12.11%, and 12.10%, respectively. With the increase in Al substitution, the temperature corresponding to the removal of structural hydroxyl groups in the goethite increases. The temperatures for the removal of structural hydroxyl groups in G-0, G-5, G-10, G-15, G-20, and G-30 are approximately ~275 °C, ~268 °C, ~272 °C, ~292 °C, ~321 °C, and ~333 °C, respectively (Figure 6b), suggesting that Al isomorphous substitution possibly enhanced the bonding force of structural hydroxyl in goethite.

3.4. VSWIR Characteristics of Synthetic Iron Hydroxides

This study primarily investigates Fe^{3+} electronic transitions in the 300–1000 nm range. The VSWIR absorptions at 400–450 nm, 480–550 nm, 640–730 nm, and 850–1000 nm are contributed by $^6A_1(^6S)\rightarrow{}^4A_1(^4G)$, $^6A_1(^6S) + {}^6A_1(^6S)\rightarrow{}^4T_1(^4G) + {}^4T_1(^4G)$, $^6A_1(^6S)\rightarrow{}^4T_2(^4G)$,

and $^6A_1(^6S)\rightarrow^4T_1(^4G)$, respectively (Table 2). Additionally, VSWIR absorption at ~1400 nm is contributed by hydroxyl (OH) groups of iron hydroxides, and the absorption at around 1910 nm corresponds to the combination tone of molecular water (H_2O) bending (δ) and hydroxyl stretching (ν) vibrations. The present study suggests that the variations in the VSWIR band positions at 420 nm (P420), 480 nm (P480), 650 nm (P650), 900 nm (P900), and 1400 nm (P1400) are essentially related to Al substitution in goethite and ferrihydrite.

Table 2. Attribution of Visible Infrared Reflectance Absorptions for iron oxides [32,33].

VSWIR Range/nm	Wavelength/nm	Attribution	Related Minerals
360–380	360–380	$^6A_1(^6S)\rightarrow^4E(^4D)$	Goethite, lepidocrocite, maghemite, hematite
400–450	420	$^6A_1(^6S)\rightarrow^4E$, $^4A_1(^4G)$	Goethite, lepidocrocite, maghemite, hematite, ferrihydrite
480–550	500 550	$^6A_1(^6S)$ + $^6A_1(^6S)\rightarrow^4T_1(^4G)$ + $^4T_1(^4G)$	Goethite, lepidocrocite, ferrihydrite Hematite
640–730	650 700	$^6A_1(^6S)\rightarrow^4T_2(^4G)$	Goethite, hematite Lepidocrocite, ferrihydrite
850–1000	850 920 940 960	$^6A_1(^6S)\rightarrow^4T_1(^4G)$	Hematite Goethite Ferrihydrite Lepidocrocite

3.4.1. Ferrihydrite

The VSWIR spectra of ferrihydrite samples exhibit broader and smoother absorption band shapes. With an increase in Al substitution, the absorption band positions of $^6A_1(^6S)\rightarrow^4T_1(^4G)$ at ~900 nm shift from 935 nm to 918 nm, and the absorption band positions of the first overtone related to OH stretching vibrations (P1400) shift towards 1429 nm to 1426 nm (Figure 7a–c). The full width at half-maximum of the absorption band around 900 nm (FWHM900) decreases from 372 nm to 359 nm, and the asymmetry of the absorption band around 1400 nm (AS1400) increases from 0.37 to 0.42 (Figure S1). However, other spectral parameters show poor correlations with increasing Al substitution in ferrihydrite (Figure S1).

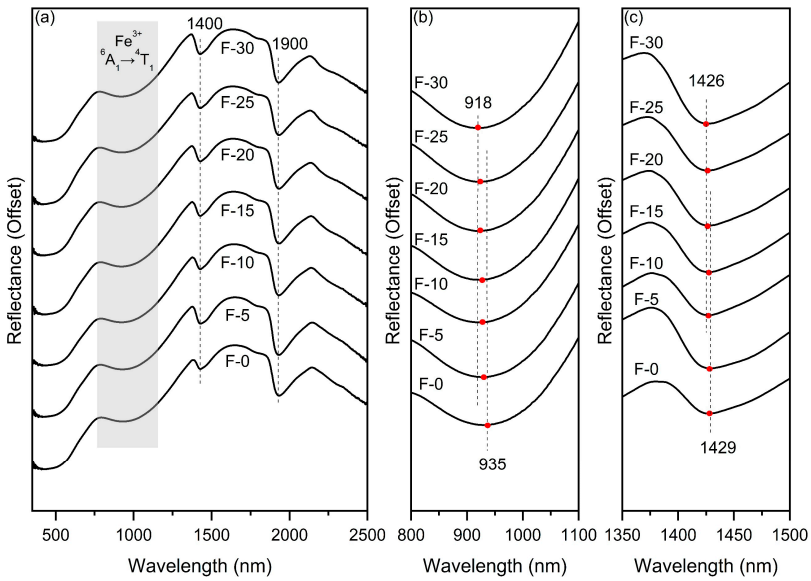

Figure 7. VSWIR spectra of Al-substituted ferrihydrite in wavelength range of 350–2500 nm (**a**), 800–1100 nm (**b**), and 1350–1500 nm (**c**).

3.4.2. Goethite

In the VSWIR reflectance spectra of Al-substituted goethite, variations in the depths and positions of the characteristic absorption are observed, corresponding to different degrees of Al substitution (Figure 8a). The VSWIR spectra of different Al-substituted goethite samples exhibit narrower and sharper absorption bands (Figure 8a). With an increase in Al substitution, the absorption depths at 420 nm (D420) decrease from 0.72 to 0.66, while the absorption depths at 480 nm (D480) decrease from 0.69 to 0.64 (Figure S2a,b). However, the correlation between P420 and P480 and the degree of Al substitution is relatively weak. P650 and P900 show varying degrees of shifts with the extent of Al substitution in goethite, i.e., a higher Al substitution leads to an increase in P650 from 655 nm to 660 nm, and P900 shifts from 930 nm to 960 nm (Figure 8b,c). Moreover, the asymmetry of the absorption band around 900 nm (AS900) increases from 0.88 to 1.05 (Figure S2f).

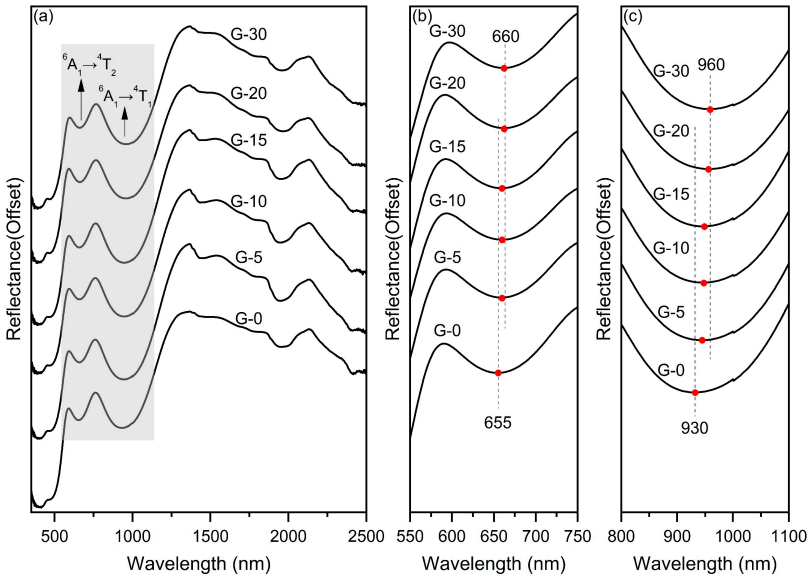

Figure 8. VSWIR spectra of Al-substituted goethite in wavelength range of 350–2500 nm (**a**), 550–750 nm (**b**), and 800–1100 nm (**c**).

4. Discussion

4.1. The Effect of Al Substitution in the Structure of Goethite and Ferrihydrite

4.1.1. Al-Substituted Ferrihydrite

Ferrihydrite is an unstable iron hydroxide [1–3,14–16]; accordingly, most of the Al-substituted ferrihydrite is composed of poorly crystallized 2 to 6 nm particles (Figure 1). The significant difference between the radii of Fe and Al could induce a large lattice distortion in ferrihydrite. To alleviate the strain of a distorted lattice, the ferrihydrite with a higher degree of Al substitution tends to have larger amounts of vacancies, and the abundance of structural protons also increases concomitantly to make the charge balanced [31,34]. As a result, the increase in structural water in Al-substituted ferrihydrite (Figure 6a) is possibly derived from hydroxyl groups induced by the Al substitution.

The TG data suggest that increasing Al substitution leads to an increase in the content of hydroxyl groups and structural water in ferrihydrite (Figure 6a). Previous studies have attributed similar phenomena in ferrihydrite to cationic vacancy defects in the structure [31,34,35].

4.1.2. Al-Substituted Goethite

Given that Al^{3+} (0.53 Å) has a smaller ionic radius relative to Fe^{3+} (0.65 Å), the internal equilibrium of the $Fe(O, OH)_6$ octahedra tends to be adjusted through contraction and distortion when Al^{3+} ions are incorporated and occupy positions originally held by Fe^{3+}.

Consequently, Al^{3+} substitution tends to lead to a reduction in the interplanar spacing (d-values) of the goethite, as is demonstrated by the gradual shift of characteristic diffractions towards high-angle 2θ angles (Figure 5b,c). In adition, Al^{3+} substitution may also lead to a disordered lattice with lower crystallinity and smaller crystals [1,2]. In contrast, the coincident increase in dehydroxylation temperatures with Al substitution in goethite (Figure 6b) can be attributed to the higher affinity constants and stronger bonding forces of Al-OH relative to Fe-OH [21,36].

4.2. Calculating the Al Substitution in Iron Hydroxides with Spectral Parameters

The absorption bands of iron hydroxides in the VSWIR range have been attributed to Fe^{3+} electronic transitions, including transitions derived from the Fe^{3+} ligand field (300–1000 nm) and ligand-to-metal charge transfer (LMCT, <270 nm) [37]. The Fe^{3+} ligand field transitions are occasionally influenced by electron exchange coupling, occurring between neighboring octahedral and tetrahedral coordination sites of Fe^{3+} cations [31,32,37,38]. Fe^{3+} electron pair transition is the result of the simultaneous excitation of adjacent Fe^{3+} centers [38]. However, the energy of ligand-to-metal charge transfer is often higher than most ligand field transitions (<270 nm), thus its absorption feature cannot be observed in VSWIR spectra [37].

4.2.1. Quantitative Spectral Analysis

The VSWIR spectra of different degrees of Al-substituted ferrihydrite display variations in absorption band positions at 900 nm (P900) and 1400 nm (P1400) (Figure 9a,b). As the Al substitution increases, both P900 and P1400 shift towards shorter wavelengths (Figure 7b,c). The absorption band at 1400 nm corresponds to the first overtone of the stretching vibration related to hydroxyl groups (-OH). The thermogravimetric (TG) analyses indicate that the incorporation of Al increases the concentration of hydroxyl groups in ferrihydrite (Figure 6a). Simultaneously, the absorption band depth at ~1400 nm (D1400) in the VSWIR spectra of the goethite series samples shows a gradual increase with an increase in Al substitution (Figure S1f). Short-wave infrared bands due to the Al-OH stretching overtone are observed as a single band at 1410 nm, and the Fe-OH stretching overtone occurs at 1430 nm [39]. Changes in the coordination environment and relative content of Al-OH and Fe-OH alter the band positions of the first overtone vibrations related to OH at 1400 nm. Through simple linear analysis, the relationship between Al substitution and P900, P1400 can be expressed as follows:

$$\mathrm{P900} = -0.43 \times \mathrm{Al}(\%) + 931, \quad R^2 = 0.78 \tag{1}$$

$$\mathrm{P1400} = -0.07 \times \mathrm{Al}(\%) + 1428, \quad R^2 = 0.59 \tag{2}$$

Al(%) ranges from 0 to 31.8.

The variations in the VSWIR absorption at 650 nm (P650) and 900 nm (P900), which correspond to $^6A_1 \rightarrow {}^4T_2$ and $^6A_1 \rightarrow {}^4T_1$ ligand field transitions, respectively, are suggested to be associated with the degrees of Al substitution (Figure 8a). Both P650 and P900 shift towards longer wavelengths as the Al substitution increases (Figures 8b,c and 9c,d), which is distinct from the ferrihydrite series. Through simple linear analysis, the functional relationship between Al substitution and P650, P900 can be expressed as follows:

$$\mathrm{P650} = 0.42 \times \mathrm{Al}(\%) + 657, \quad R^2 = 0.62 \tag{3}$$

$$\mathrm{P900} = 2.29 \times \mathrm{Al}(\%) + 936, \quad R^2 = 0.82 \tag{4}$$

Al(%) ranges from 0 to 11.2.

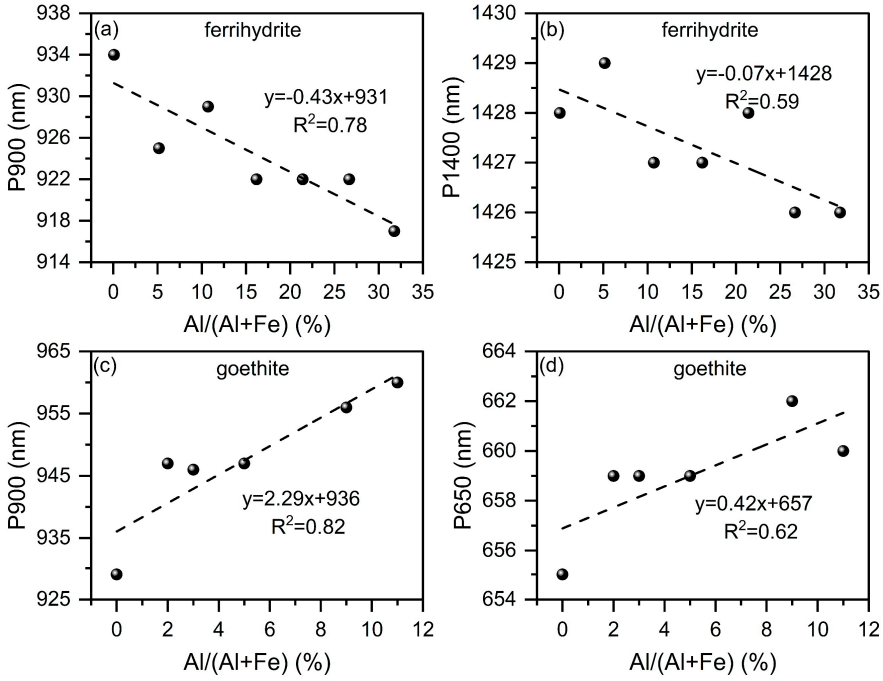

Figure 9. The correlation (**a**,**b**) between the substitution amount of Al in ferrihydrite and P900, P1400; the correlation (**c**,**d**) between the substitution amount of Al in goethite and P900, P650.

The experimental results suggest that the incorporation of Al in iron hydroxides could reduce the interlayer spacing in goethite, increase the hydroxyl and structural water content, and induce distortion in the $Fe(O, OH)_6$ octahedra, which is consistent with previous observations [1,2]. In addition, the distortion in the $Fe(O, OH)_6$ octahedra reduces crystal symmetry, thus altering the Fe^{3+} ligand field transitions and causing shifts in the band positions of P650 and P900 between goethite and ferrihydrite. It is suggested that the opposite trends in P900 between goethite and ferrihydrite result from the type and content of ligand bound to the iron atom [40,41], but the explicit coordination environment of Fe^{3+} cation in goethite and ferrihydrite with an increase in Al is still unclear. Moreover, the variations in the spectral parameters P480 and P500 of Al-substituted goethite and ferrihydrite associated with the $^6A_1(^6S)+^6A_1(^6S)\rightarrow^4T_1(^4G)+^4T_1(^4G)$ electron pair transition are insignificant, whereas Al substitution may modify the Fe^{3+}-Fe^{3+} magnetic coupling between the shared octahedra and influence electron pair transitions.

Previous studies suggested that particle size could affect the spectral behavior of goethite at 900 nm [42]. In this study, the particle size of the synthesized Al-goethite is consistently less than 2 μm (Figure 2), corresponding to that of iron hydroxide particles within soils and weathering crusts typically ranging from tens of nanometers to a few micrometers [43–46]. The comparison results indicate that size variation has a minimal influence on the VSWIR spectral features (e.g., P650 and P900) of goethite when the particle size < 30 μm (Table 3, Figure 10). Consequently, VSWIR spectra are feasible for the determination of Al substitution in iron hydroxides within weathering crusts and soils.

Table 3. Particle sizes, the position of the absorption feature around 650 nm (P650), and the position of the absorption feature around 900 nm (P900) of goethite.

Sample	Resources	Particle Size (μm)	P650	P900	References
GthA	Synthetic goethite	<20 μm	-	930	[43]
GthB	Goethite from Marra Mamba deposit	<20 μm	-	931	[43]
Gth1	Synthetic goethite	~0.14 μm	655	929	-
Gth2	Synthetic goethite	~0.07 μm	654	929	-

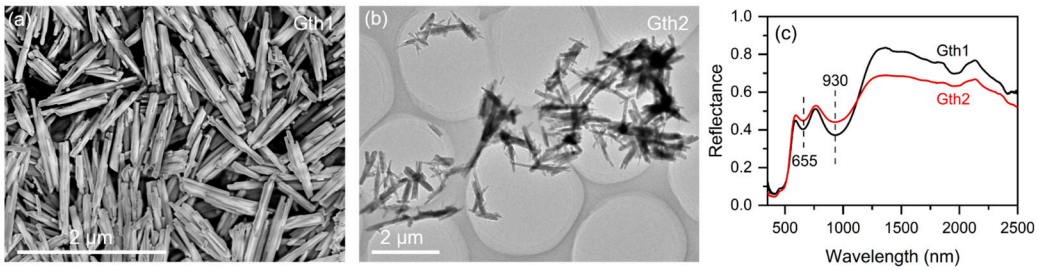

Figure 10. SEM image of Gth1 (**a**), TEM image of Gth2 (**b**), and VSWIR spectra of Gth1 and Gth2 (**c**).

In addition, the influence from other phases, e.g., hematite, in a mixture could also affect the accuracy of the estimated extent of Al substitution using the VSWIR spectral feature P900 (Figure 11). Notably, the presence of hematite poses insignificant changes in P650 and P1400 (Figure 12). Therefore, we suggest that the extent of Al substitution in goethite and ferrihydrite can be identified based on the positions of the absorption bands at 650 nm (P650) and 1400 nm (P1400), respectively.

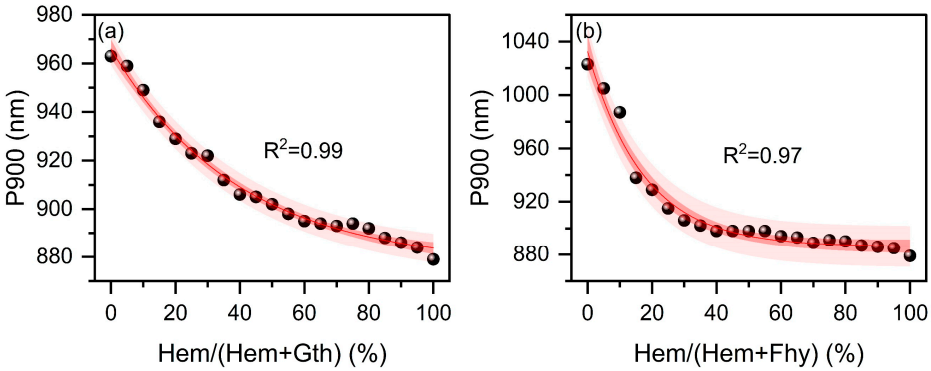

Figure 11. Correlation between spectral parameters P900 of VSWIR spectra with continuum removed of Hem-Gth (**a**), and Hem-Fhy (**b**).

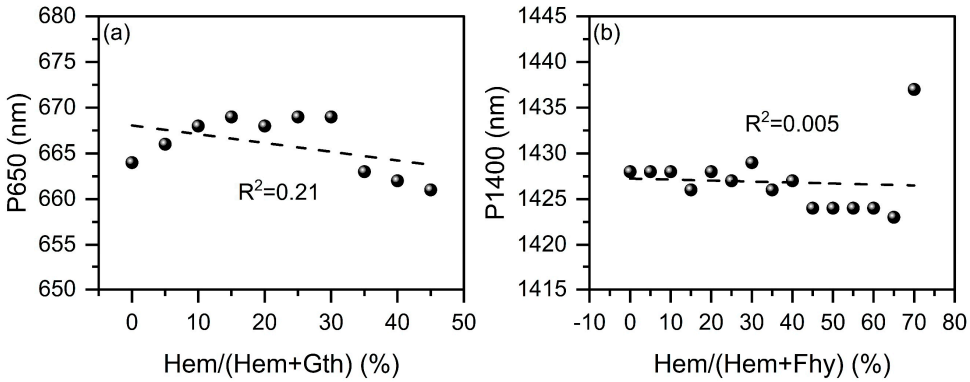

Figure 12. The correlation between spectral parameters P650 and Hem/(Hem+Gth) (**a**), and the correlation between P1400 and Hem/(Hem+Fhy) (**b**).

4.2.2. Analysis of the Effect of Al Substitution on Fe^{3+} Electronic Transitions

Due to the broad and overlapping absorption bands of Fe^{3+} in the VSWIR spectrum, with weak spectral fingerprint characteristics, previous studies have likely overlooked the role of changes in 400–450 nm, 480–550 nm, 640–730 nm, and 850–1000 nm band absorption intensity in the complete VSWIR spectra [32,33]. A peak deconvolution on the Fe^{3+} absorption range in the spectrum of iron hydroxides can reveal the changes in each peak of different degrees of Al substitution.

Four fitted absorption peaks were resolved by PeakFit from each spectrum (Figures 13a–f and 14a–f), with fitting correlation coefficients (R^2) all exceeding 0.98, indicating a significant fitting effect (Table S1). The peak fitting results show that the trend of the absorption band positions at ~650 nm and ~900 nm for Al-substituted iron hydroxides with the change of Al substitution amount is consistent with the results in Section 3.4, indicating that Al substitution leads to a shift in the absorption band positions of the VSWIR spectrum (Figures 13 and 14). An analysis of the parameters from the VSWIR peak-fitting spectra revealed that the intensity (Amplitude in PeakFit results) of the absorption peaks (Amp545 of ferrihydrite, Amp497 of goethite) associated with the $^6A_1(^6S)+^6A_1(^6S)\rightarrow^4T_1(^4G)+\ ^4T_1(^4G)$ electron pair transition showed the best correlation with changes in Al substitution (Figures 15c and 16b). The fitting results demonstrated a decrease in the intensity of the absorption peaks corresponding to electron pair transitions with increasing Al substitution. This suggests that the energy generated by the simultaneous excitation of two adjacent magnetically coupled Fe^{3+} cations decreases with increasing Al substitution.

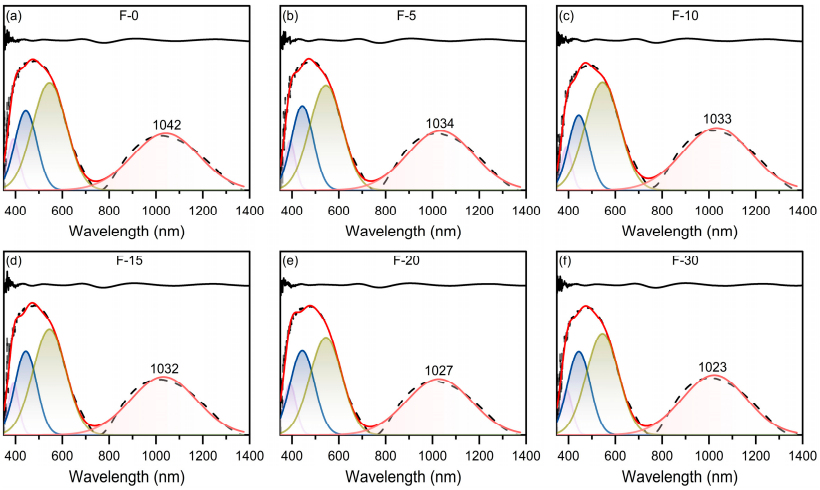

Figure 13. Four-component peak fit of simulated spectrum of ferrihydrite (**a**–**f**). Gray dotted line: spectrum, red line: sum of fit components, purple: $^6A_1(^6S)\rightarrow^4E(^4D)$, blue: $^6A_1(^6S)\rightarrow^4E$, $^4A_1(^4G)$, chartreuse: $^6A_1(^6S)+^6A_1(6S)\rightarrow^4T_1(^4G)+\ ^4T_1(^4G)$, light red: $^6A_1(^6S)\rightarrow^4T_1(^4G)$, black: residuals (at top of panels).

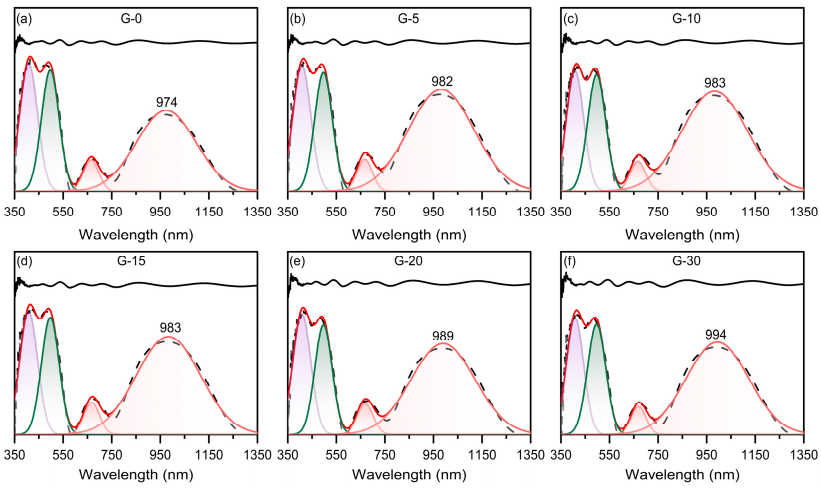

Figure 14. Four-component peak fit of simulated spectrum of goethite (**a**–**f**). Gray dotted line: spectrum, red line: sum of fit components, purple: $^6A_1(^6S)\rightarrow^4E$, $^4A_1(^4G)$, green: $^6A_1(^6S)+^6A_1(^6S)\rightarrow^4T_1(^4G)+\ ^4T_1(^4G)$, red: $^6A_1(^6S)\rightarrow^4T_2(^4G)$, light red: $^6A_1(^6S)\rightarrow^4T_1(^4G)$, black: residuals (at top of panels).

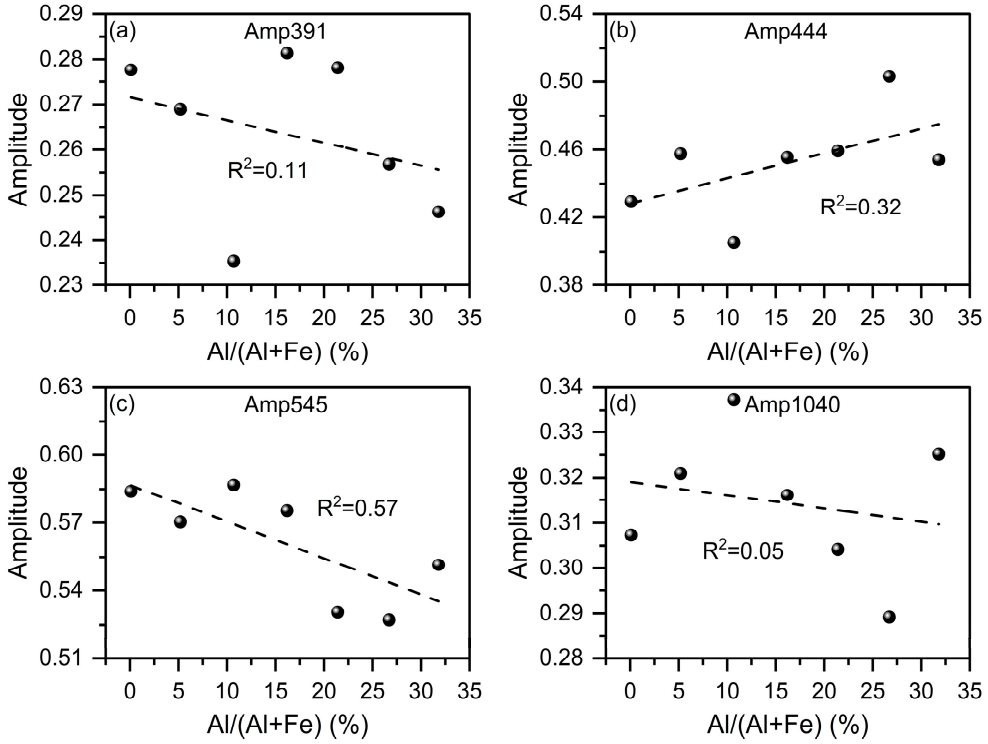

Figure 15. The simulated amplitude of the spectrum of Al-substituted ferrihydrite at the bands of 391 nm (**a**), 444 nm (**b**), 545 nm (**c**), and 1040 nm (**d**). Amp: amplitude herein refers to the absorption intensities of the corresponding band.

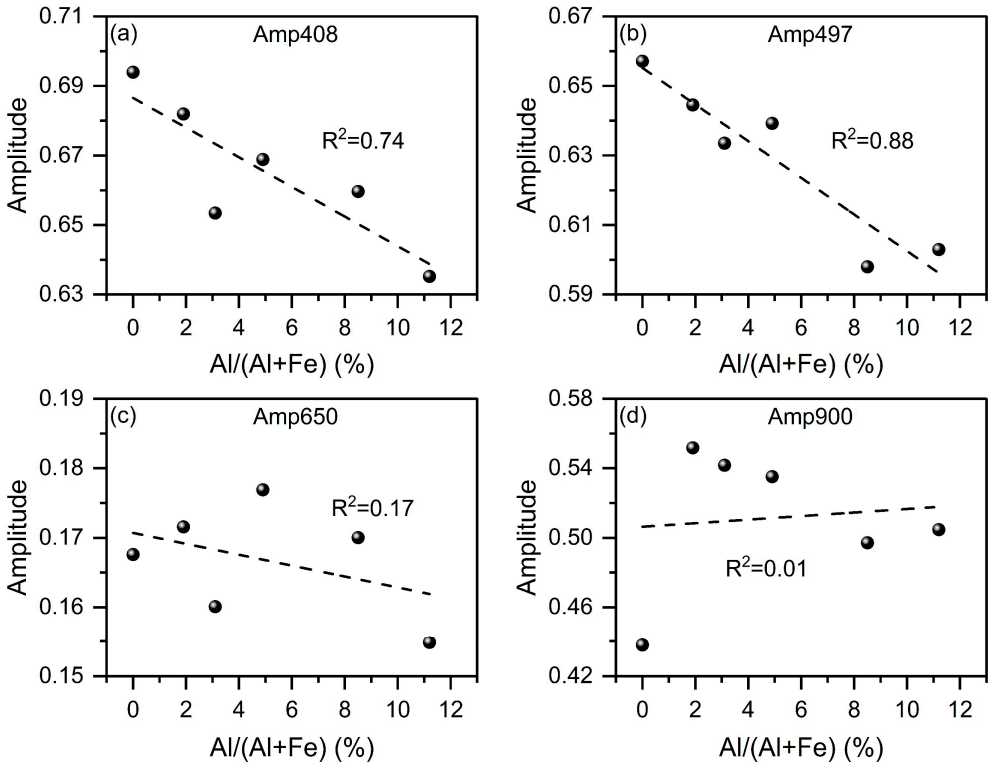

Figure 16. The simulated amplitude of the spectrum of Al-substituted goethite at the bands of 408 nm (**a**), 497 nm (**b**), 650 nm (**c**), and 900 nm (**d**). Amp: amplitude herein refers to the absorption intensities of the corresponding band.

The absorption intensities of $^6A_1(^6S)\rightarrow^4E$, $^4A_1(^4G)$ ligand field transitions have a good correlation with the absorption intensity of $^6A_1(^6S)$ + $^6A_1(^6S)\rightarrow^4T_1(^4G)$ + $^4T_1(^4G)$ (Figure 17b,d). Among them, in the ferrihydrite series, Amp444 is negatively correlated with Amp545, while in the goethite series, Amp408 is positively correlated with Amp497. The absorption peak at 391 nm may be affected by the relatively high noise, resulting in a weaker correlation with the absorption peak intensity related to the electron pair transition (Figure 17a). Therefore, we propose that the incorporation of Al into the crystal lattice induces distortion in the distance between Fe and (O, OH) in iron hydroxides, thus reducing crystal symmetry. The energy associated with the simultaneous excitation of adjacent Fe^{3+} cations through magnetic coupling decreases. Consequently, the characteristic at the band of 480–550 nm displays a weakened absorption intensity related to the $^6A_1(^6S)$ + $^6A_1(^6S)\rightarrow^4T_1(^4G)$ + $^4T_1(^4G)$ transition process. Simultaneously, transitions between states on the Fe (3d) atom orbitals, which arise from the different possible electronic configurations caused by changes in the coordination environment, lead to shifts in the observed positions of VSWIR spectral absorption bands. However, the specific mechanisms underlying these changes remain unclear and warrant further investigation.

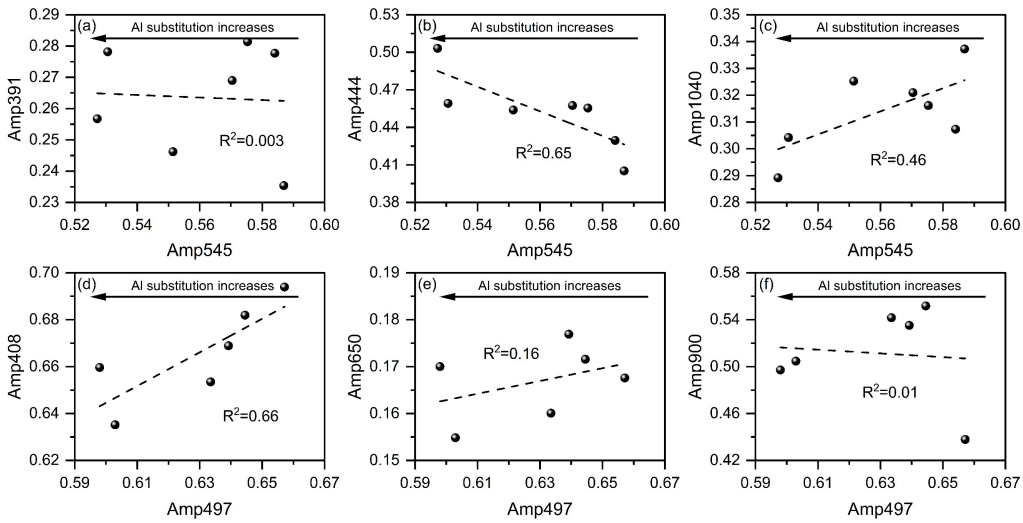

Figure 17. The relationship (**a**–**c**) between the absorption peak intensity of ligand field transitions ($^6A_1(^6S)\rightarrow^4E$, $^4A_1(^4G)$, $^6A_1(^6S)\rightarrow^4T_2(^4G)$, $^6A_1(^6S)\rightarrow^4T_1(^4G)$) in simulated spectra of goethite and the absorption peak intensity of $^6A_1(^6S)$+$^6A_1(^6S)\rightarrow^4T_1(^4G)$+ $^4T_1(^4G)$; The relationship (**d**–**f**) between the absorption peak intensity of ligand field transitions ($^6A_1(^6S)\rightarrow^4E(^4D)$, $^6A_1(^6S)\rightarrow^4E$, $^4A_1(^4G)$, $^6A_1(^6S)\rightarrow^4T_1(^4G)$) in simulated spectra of ferrihydrite and the absorption peak intensity of $^6A_1(^6S)$+$^6A_1(^6S)\rightarrow^4T_1(^4G)$+ $^4T_1(^4G)$. Amp: amplitude.

5. Conclusions

This study presents systematic VSWIR spectral characteristics of a series of synthesized Al-substituted goethite and ferrihydrite samples.

(1) Empirical relationships between VSWIR spectral parameters (P650, P900, and P1400) and the Al substitution of goethite and ferrihydrite were established. The absorption band positions and intensities of VSWIR spectra can be utilized for the semi-quantitative determination of Al substitution in iron hydroxides when the Al substitution levels range from 0 to 11.2% in goethite and 0 to 31.8% in ferrihydrite. The above results currently apply only to the investigated synthesized samples and further research is needed to apply them to rock samples.

(2) In the identification of Al substitution in individual minerals, P900 proves to be the most efficient spectral parameter. Conversely, P650 and P1400 can be employed to evaluate the Al substitution levels in goethite and ferrihydrite, respectively, when other iron hydroxide minerals (e.g., hematite) are present.

(3) The absorption band intensity in the 480–550 nm range, attributed to the $^6A_1(^6S)$ + $^6A_1(^6S) \rightarrow {}^4T_1(^4G)$ + $^4T_1(^4G)$ transition, is sensitive to changes in Al substitution, providing a reliable metric for assessing the extent of Al substitution in iron hydroxides.

Supplementary Materials: The following supporting information can be downloaded at: https://www.mdpi.com/article/10.3390/min14060618/s1, Figure S1: The correlation (a–d) between the substitution amount of Al in ferrihydrite and FWHM900, FWHM1400; AS900 and AS1400; Figure S2: The correlation (a–f) between the substitution amount of Al in goethite and D420, D480, FWHM650, FWHM900, AS650 and AS900; Figure S3: The correlation (a–b) between the Al substitution of ferrihydrite and P900, P1400 with continuum removal; Figure S4: The correlation (a–b) between the Al substitution of goethite and P900, P650 with continuum removal; Table S1: VSWIR spectral peak-fitting results of Al substitution for goethite and ferrihydrite.

Author Contributions: Data curation, X.Q., X.L., J.Z. (Jianxi Zhu), M.H., and L.L.; Project administration, W.T. and H.H.; Resources, J.Z. (Jingwen Zhou), and X.L.; Supervision, W.T. and H.H.; Writing—original draft, K.C. and W.T.; Writing—review and editing, K.C., X.Q., and W.T. All authors have read and agreed to the published version of the manuscript.

Funding: This research was funded by the Strategic Priority Research Program of the Chinese Academy of Sciences, grant number XDA0430205; the National Natural Science Foundation of China, grant numbers 41921003 and 42022012; the National Key R&D Program of China, grant number 2021YFC2901701; the Youth Innovation Promotion Association CAS, grant number 2023369; Science and Technology Planning of Guangdong Province, China, grant number 2023B1212060048; and the Technology & Geology Planning Project of Jiangxi Province, China, grant number 2023KDG01006.

Data Availability Statement: The visible short-wave infrared reflectance spectroscopy (VSWIR) of Al-substituted ferrihydrite and Al-substituted goethite are available in an external repository via Mendeley Data (doi: 10.17632/684bwg68w2.1).

Acknowledgments: The authors sincerely thank three anonymous reviewers for their critical reviews and constructive comments, which have improved the manuscript. This is contribution No.IS-3528 from GIGCAS.

Conflicts of Interest: The authors declare no conflicts of interest.

References

1. Cornell, R.M.; Schwertmann, U. *The Iron Oxides: Structure, Properties, Reactions, Occurrences, and Uses*; Wiley-VCH Weinheim: Weinheim, Germany, 2003; Volume 664.
2. Jiang, Z.; Liu, Q.; Roberts, A.P.; Dekkers, M.J.; Barrón, V.; Torrent, J.; Li, S. The magnetic and color reflectance properties of hematite: From Earth to Mars. *Rev. Geophys.* **2022**, *60*, e2020RG000698. [CrossRef]
3. Meng, X.; Li, G.K.; Long, X.; Li, S.; Ji, J. Quantifying Soil Goethite/Hematite Ratios: A New Method Based on Diffuse Reflectance Spectra. *Geophys. Res. Lett.* **2023**, *50*, e2022GL102280. [CrossRef]
4. Hu, P.; Jiang, Z.; Liu, Q.; Helslop, D.; Roberts, A.P.; Torrent, J.; Barrón, V. Estimating the concentration of aluminum-substituted hematite and goethite using diffuse reflectance spectrometry and rock magnetism: Feasibility and limitations. *J. Geophys. Res. Solid Earth* **2016**, *121*, 4180–4194. [CrossRef]
5. Wang, X.; Yang, K.; Sun, S.; Xu, J.; Li, Y.; Liu, F.; Feng, X. The structure and composition of ferrihydrite and its environmental geochemical behaviors. *Earth Sci. Front.* **2011**, *18*, 339–347.
6. Felix-Henningsen, P. Paleosols on Pleistocene dunes as indicators of paleo-monsoon events in the Sahara of East Niger. *Catena* **2000**, *41*, 43–60. [CrossRef]
7. Kämpf, N.; Schwertmann, U. Goethite and hematite in a climosequence in southern Brazil and their application in classification of kaolinitic soils. *Geoderma* **1983**, *29*, 27–39. [CrossRef]
8. Bolanz, R.M.; Kiefer, S.; Göttlicher, J.; Steininger, R. Hematite (α-Fe_2O_3)—A potential Ce^{4+} carrier in red mud. *Sci. Total Environ.* **2018**, *622*, 849–860. [CrossRef]
9. Hao, Q.; Oldfield, F.; Bloemendal, J.; Torrent, J.; Guo, Z. The record of changing hematite and goethite accumulation over the past 22 Myr on the Chinese Loess Plateau from magnetic measurements and diffuse reflectance spectroscopy. *J. Geophys. Res. Solid Earth* **2009**, *114*, B12101. [CrossRef]
10. Long, X.; Ji, J.; Balsam, W. Rainfall-dependent transformations of iron oxides in a tropical saprolite transect of Hainan Island, South China: Spectral and magnetic measurements. *J. Geophys. Res. Earth Surf.* **2011**, *116*, F0315. [CrossRef]

11. Lyons, R.; Tooth, S.; Duller, G.A. Late Quaternary climatic changes revealed by luminescence dating, mineral magnetism and diffuse reflectance spectroscopy of river terrace palaeosols: A new form of geoproxy data for the southern African interior. *Quat. Sci. Rev.* **2014**, *95*, 43–59. [CrossRef]
12. Tan, W.; Qin, X.R.; Liu, J.C.; Zhou, M.F.; He, H.P.; Wang, C.Y.; Huang, J.; Zhu, J.X.; Yao, Y.Z.; and Cudahy, T. Feasibility of visible short-wave infrared reflectance spectroscopy to characterize regolith-hosted rare earth element mineralization. *Econ. Geol.* **2022**, *117*, 495–508. [CrossRef]
13. Manceau, A.; Gates, W.P. Incorporation of Al in Iron Oxyhydroxides: Implications for the Structure of Ferrihydrite. *Clay Miner.* **2013**, *48*, 481–489. [CrossRef]
14. Pinney, N.; Morgan, D. Thermodynamics of Al-Substitution in Fe-Oxyhydroxides. *Geochim. Et Cosmochim. Acta* **2013**, *120*, 514–530. [CrossRef]
15. Adams, F.T.; Machesky, M.L.; Kabengi, N. Surface Complexation Modeling Approach for Aluminum-Substituted Ferrihydrites. *ACS Earth Space Chem.* **2021**, *5*, 1355–1362. [CrossRef]
16. Bompoti, M.N.; Cruz-Hernández, Y.; Chrysochoou, M.; Machesky, M.L. Interfacial Properties of Al-Ferrihydrites: Surface Complexation Modeling as a Probe of Surface Structure. *ACS Earth Space Chem.* **2022**, *6*, 1717–1724. [CrossRef]
17. Jentzsch, T.L.; Penn, R.L. Influence of aluminum doping on ferrihydrite nanoparticle reactivity. *J. Phys. Chem. B* **2006**, *110*, 11746–11750. [CrossRef]
18. Morris, R.V.; Schulze, D.G.; Lauer, H.V., Jr.; Agresti, D.G.; Shelfer, T.D. Reflectivity (visible and near IR), Mössbauer, static magnetic, and X ray diffraction properties of aluminum-substituted hematites. *J. Geophys. Res. Planets* **1992**, *97*, 10257–10266. [CrossRef]
19. Liu, H.; Chen, T.; Zou, X.; Qing, C.; Frost, R.L. Effect of Al content on the structure of Al-substituted goethite: A micro-Raman spectroscopic study. *J. Raman Spectrosc.* **2013**, *44*, 1609–1614. [CrossRef]
20. Jiang, S.; Yan, X.; Peacock, C.L.; Zhang, S.; Li, W.; Zhang, J.; Feng, X.; Liu, F.; Yin, H. Adsorption of Cr (VI) on Al-substituted hematites and its reduction and retention in the presence of Fe^{2+} under conditions similar to subsurface soil environments. *J. Hazard. Mater.* **2020**, *390*, 122014. [CrossRef]
21. Ruan, H.; Frost, R.L.; Kloprogge, J.T.; Duong, L. Infrared spectroscopy of goethite dehydroxylation. II. Effect of aluminium substitution on the behaviour of hydroxyl units. *Spectrochim. Acta Part A Mol. Biomol. Spectrosc.* **2002**, *58*, 479–491. [CrossRef]
22. Cismasu, A.C.; Michel, F.M.; Stebbins, J.F.; Levard, C.; Brown, G.E., Jr. Properties of impurity-bearing ferrihydrite I. Effects of Al content and precipitation rate on the structure of 2-line ferrihydrite. *Geochim. Et Cosmochim. Acta* **2012**, *92*, 275–291. [CrossRef]
23. Fang, Q.; Hong, H.; Zhao, L.; Kukolich, S.; Yin, K.; Wang, C. Visible and near-infrared reflectance spectroscopy for investigating soil mineralogy: A review. *J. Spectrosc.* **2018**, *2018*, 3168974. [CrossRef]
24. Jones, S.; Herrmann, W.; Gemmell, J.B. Short wavelength infrared spectral characteristics of the HW horizon: Implications for exploration in the Myra Falls volcanic-hosted massive sulfide camp, Vancouver Island, British Columbia, Canada. *Econ. Geol.* **2005**, *100*, 273–294. [CrossRef]
25. Nocita, M.; Stevens, A.; Noon, C.; van Wesemael, B. Prediction of soil organic carbon for different levels of soil moisture using Vis-NIR spectroscopy. *Geoderma* **2013**, *199*, 7–42. [CrossRef]
26. dos Reis Salles, R.; de Souza Filho, C.R.; Cudahy, T.; Vicente, L.E.; Monteiro, L.V.S. Hyperspectral remote sensing applied to uranium exploration: A case study at the Mary Kathleen metamorphic-hydrothermal U-REE deposit, NW, Queensland, Australia. *J. Geochem. Explor.* **2017**, *179*, 36–50. [CrossRef]
27. Böhm, J. Über Aluminium-und Eisenhydroxyde. I. *Z. Für Anorg. Und Allg. Chem.* **1925**, *149*, 203–216. [CrossRef]
28. Chen, R.; Jakes, K.A.; Foreman, D.W. Peak-fitting analysis of cotton fiber powder X-ray diffraction spectra. *J. Appl. Polym. Sci.* **2004**, *93*, 2019–2024. [CrossRef]
29. Han, P. Application of Peakfit in FT-IR spectrum fitting and chemical composition analysis of M-type ferrite. *J. Shenyang Inst. Technol.* **2021**, *40*, 66–70.
30. Liu, J.; He, H.; Michalski, J.R.; Cuadros, J.; Yao, Y.; Tan, W.; Qin, X.; Li, S.; Wei, G. Reflectance spectroscopy applied to clay mineralogy and alteration intensity of a thick basaltic weathering sequence in Hainan Island, South China. *Appl. Clay Sci.* **2021**, *201*, 105923. [CrossRef]
31. Michel, F.M.; Barrón, V.; Torrent, J.; Morales, M.P.; Serna, C.J.; Boily, J.F.; Liu, Q.; Ambrosini, A.; Cismasu, A.C.; Brown, G.E., Jr. Ordered ferrimagnetic form of ferrihydrite reveals links among structure, composition, and magnetism. *Proc. Natl. Acad. Sci. USA* **2010**, *107*, 2787–2792. [CrossRef] [PubMed]
32. Scheinost, A.; Chavernas, A.; Barrón, V.; Torrent, J. Use and limitations of second-derivative diffuse reflectance spectroscopy in the visible to near-infrared range to identify and quantify Fe oxide minerals in soils. *Clays Clay Miner.* **1998**, *46*, 528–536. [CrossRef]
33. Morris, R.V.; Lauer, H.V., Jr.; Lawson, C.A.; Gibson, E.; Knace, G.A.; Stewart, C. Spectral and other physicochemical properties of submicron powders of hematite (α-Fe_2O_3), maghemite (γ-Fe_2O_3), magnetite (Fe_3O_4), goethite (α-FeOOH), and lepidocrocite (γ-FeOOH). *J. Geophys. Res. Solid Earth* **1985**, *90*, 3126–3144. [CrossRef] [PubMed]
34. Li, W.; Wang, L.; Liu, F.; Liang, X.; Feng, X.; Tan, W.; Zheng, L.; Yin, H. Effects of Al^{3+} doping on the structure and properties of goethite and its adsorption behavior towards phosphate. *J. Environ. Sci.* **2016**, *45*, 18–27. [CrossRef] [PubMed]
35. Liang, Y. Mechanisms of Lead Adsorption on Al-Substituted Iron Oxides and CD-MUSIC Modeling. Ph.D. Thesis, Huazhong Agricultural University, Wuhan, China, 2022.

36. Han, J.; Katz, L.E. Capturing the variable reactivity of goethites in surface complexation modeling by correlating model parameters with specific surface area. *Geochim. Et Cosmochim. Acta* **2019**, *244*, 248–263. [CrossRef]
37. Sherman, D.M.; Waite, T.D. Electronic spectra of Fe^{3+} oxides and oxide hydroxides in the near IR to near UV. *Am. Mineral.* **1985**, *70*, 1262–1269.
38. Schugar, H.J.; Rossman, G.R.; Thibeault, J.; Gray, H.B. Simultaneous pair electronic excitations in a binuclear iron (III) complex. *Chem. Phys. Lett.* **1970**, *6*, 26–28. [CrossRef]
39. Bishop, J.; Lane, M.; Dyar, M.; Brown, A. Reflectance and emission spectroscopy study of four groups of phyllosilicates: Smectites, kaolinite-serpentines, chlorites and micas. *Clay Miner.* **2008**, *43*, 35–54. [CrossRef]
40. Burns, R.G.; Fisher, D.S. Rates of oxidative weathering on the surface of Mars. *J. Geophys. Res. Planets* **1993**, *98*, 3365–3372. [CrossRef]
41. Bishop, J.L.; Murad, E. The visible and infrared spectral properties of jarosite and alunite. *Am. Mineral.* **2005**, *90*, 1100–1107. [CrossRef]
42. Ramanaidou, E.; Wells, M.; Belton, D.; Ryan, C. Mineralogical and Microchemical Methods for the Characterization of High-Grade BIF Derived Iron Ore. *SEG Rev.* **2008**, *15*, 129–156.
43. Cudahy, T.; Ramanaidou, E. Measurement of the hematite: Goethite ratio using field visible and near-infrared reflectance spectrometry in channel iron deposits, Western Australia. *Aust. J. Earth Sci.* **1997**, *44*, 411–420. [CrossRef]
44. Huang, J.; Tan, W.; Liang, X.; He, H.; Ma, L.; Bao, Z.; Zhu, J. REE fractionation controlled by REE speciation during formation of the Renju regolith-hosted REE deposits in Guangdong Province, South China. *Ore Geol. Rev.* **2021**, *134*, 104172. [CrossRef]
45. Sanematsu, K.; Kon, Y.; Imai, A.; Watanabe, K.; Watanabe, Y. Geochemical and mineralogical characteristics of ion-adsorption type REE mineralization in Phuket, Thailand. *Miner. Depos.* **2013**, *48*, 437–451. [CrossRef]
46. Zhao, L.; Hong, H.; Fang, Q.; Yin, K.; Wang, C.; Li, Z.; Torrent, J.; Cheng, F.; Algeo, T.J. Monsoonal climate evolution in southern China since 1.2 Ma: New constraints from Fe-oxide records in red earth sediments from the Shengli section, Chengdu Basin. *Palaeogeogr. Palaeoclimatol. Palaeoecol.* **2017**, *473*, 1–15. [CrossRef]

Disclaimer/Publisher's Note: The statements, opinions and data contained in all publications are solely those of the individual author(s) and contributor(s) and not of MDPI and/or the editor(s). MDPI and/or the editor(s) disclaim responsibility for any injury to people or property resulting from any ideas, methods, instructions or products referred to in the content.